Postprint of: Kozieł S., Pietrenko-Dąbrowska A., Ubaid U., Low-Cost Modeling of Microwave Components by Means of Two-Stage Inverse/Forward Surrogates and Domain Confinement, IEEE TRANSACTIONS ON MICROWAVE THEORY AND TECHNIQUES (2021), pp. 1-14, DOI: 10.1109/TMTT.2021.3112156

Low-Cost Modeling of Microwave Components by Means of Two-Stage Inverse/Forward Surrogates and Domain Confinement

Slawomir Koziel , *Senior Member, IEEE*, Anna Pietrenko-Dabrowska , *Senior Member, IEEE*, and Ubaid Ullah , *Member, IEEE*

***Abstract*— Full-wave electromagnetic (EM) analysis is one of the most important tools in the design of modern microwave components and systems. EM simulation permits reliable evaluation of circuits at the presence of cross-coupling effects or substrate anisotropy, as well as for accounting for interactions with the immediate environment. However, repetitive analyses required by EM-driven procedures, such as parametric optimization or statistical analysis, may entail considerable computational expenditures, often prohibitive. Tackling the high-cost issue fostered the shift toward the incorporation of fast replacement models, including both physics-based surrogates and data-driven ones. While the latter is more popular and versatile, the construction of reliable approximation metamodels for microwave components is hindered by the curse of dimensionality and nonlinearity of system responses. The recent performance-driven modeling methodologies are capable of alleviating these difficulties by confining the surrogate domain to a vicinity of the optimum design manifold (i.e., the region that contains high-quality designs rather than the entire parameter space). Although setting up the model in a constrained domain requires small amounts of training data, domain definition itself requires a set of preoptimized reference designs, acquisition of which is an expensive endeavor. This work proposes a novel approach, which replaces the reference designs with a small set of random observables, thereby considerably reducing the overall cost of the model setup. Comprehensive verification involving several miniaturized microstrip structures demonstrates that our methodology is competitive to performance-driven frameworks both in terms of modeling accuracy and computational efficiency with an average savings of around 80%.**

***Index Terms*— Domain confinement, inverse models, microwave design, miniaturized components, performance-driven modeling, regression models, surrogate modeling.**

Manuscript received May 17, 2021; revised June 30, 2021 and August 4, 2021; accepted August 25, 2021. This work was supported in part by the Icelandic Center for Research (RANNIS) under Grant 217771 and in part by the National Science Center of Poland under Grant 2020/37/B/ST7/01448. *(Corresponding author: Anna Pietrenko-Dabrowska.)*

Slawomir Koziel is with the Engineering Optimization and Modeling Center, Reykjavik University, 102 Reykjavik, Iceland, and also with the Faculty of Electronics, Telecommunications and Informatics, Gdańsk University of Technology, 80-233 Gdańsk, Poland (e-mail: koziel@ru.is).

Anna Pietrenko-Dabrowska is with the Faculty of Electronics, Telecommunications and Informatics, Gdańsk University of Technology, 80-233 Gdańsk, Poland (e-mail: anna.dabrowska@pg.edu.pl).

Ubaid Ullah is with the Department of Networks and Communication Engineering, Al Ain University of Science and Technology, Abu Dhabi, UAE (e-mail: ubaid.ullah@aau.ac.ae).

Color versions of one or more figures in this article are available at https://doi.org/10.1109/TMTT.2021.3112156.

Digital Object Identifier 10.1109/TMTT.2021.3112156

I. Introduction

ELECTROMAGNETIC (EM)-driven design has become instrumental in achieving the best possible performance for the vast majority of microwave components and devices. While theoretical models (analytical [1] and equivalent network [2]) are often capable of yielding reasonable initial designs, optimization-based design closure is still necessary. The latter is most often carried out at the level of EM simulation tools. This is especially pertinent to miniaturized components featuring tightly arranged layouts, where a strong cross-coupling effect makes the equivalent network representations grossly inaccurate [3]. These issues are related to specific miniaturization techniques, e.g., transmission line folding [4], utilization of the slow wave effects (e.g., compact microwave resonant cells, CMRSs [5]), or multilayer realizations (e.g., LTCC structures [6]).

Although full-wave EM analysis ensures evaluation accuracy, it also entails considerable computational expenses. These are usually not troublesome for design verification but may become impractically high whenever repetitive simulations are necessary. The examples of relevant simulation-based tasks include, first and foremost, parameter tuning (also referred to as design closure) [7], statistical analysis [8], yield-driven design [9] (or, more generally, uncertainty quantification, UQ, [10]), global [11], [12], or multiobjective optimization (MO) [13]. It is especially the case of UQ and MO, where the computational costs may readily become prohibitive when using conventional approaches directly at the level of EM models (e.g., Monte Carlo simulation for UQ [14] or population-based nature-inspired algorithms [15]–[17] for MO or global search). A possible workaround is to employ simplified design procedures that are computationally tractable but lack accuracy (e.g., supervised parameter sweeping for geometry parameter adjustment [18] or worst case analysis for UQ [19]). In the realm of rigorous approaches, there have been a large number of methodologies developed to accelerate EM-driven procedures, including both algorithmic techniques (e.g., incorporation of adjoint sensitivities [20] or sparse Jacobian updates [21] into gradient-based routines, parallelization [22], and mesh deformation methods [23]) but also—more and more popular—surrogate-assisted solutions [24]–[29]. Among these, physics-based surrogates are most often employed in local optimization [30].

The models of this class are characterized by improved generalization capability [31], which is a result of capitalizing on the problem-specific knowledge embedded in an underlying low-fidelity representation (e.g., an equivalent circuit [32]). Popular methods include space mapping [33], manifold mapping [34], or various response correction techniques [35], [36]. Still, the versatility of physics-based modeling methods, with a notable example of space mapping, is considerably limited by the following factors. The techniques of this class require an underlying low-fidelity model, which is problem-dependent and whose quality significantly affects the performance of the entire modeling framework. Development and selection of such a model require engineering insight and, for some structures (e.g., those with strong EM cross-coupling effects), maybe problematic accuracywise. Moreover, physics-based surrogates, being, as a matter of fact, nonlinear regression models with a fixed number of degrees of freedom, do not have universal approximation capability. The latter makes it difficult to ensure the assumed predictive power of the surrogate regardless of the number of training data points involved.

Data-driven surrogates (kriging [37], Gaussian process regression [38], neural networks [39], ensemble learning [40], and support vector regression [41]) are typically applied in global optimization frameworks [12], often in combination with sequential sampling [42] or machine-learning schemes [43]. Polynomial chaos expansion (PCE) models are particularly suitable for handling UQ tasks by eliminating the need for Monte Carlo analysis [44]. Other worth noticing techniques include feature-based optimization (FBO) [45] and cognition-driven design [46], both relying on the exploitation of a specific structure of the system response (e.g., passband ripples [47] or allocation of the system resonances [48]).

It is clear that an overall replacement of expensive EM simulations by a fast surrogate would open the door to low-cost execution of all sorts of design tasks. Due to their versatility, easy access (e.g., [49] and [50]), and handling, the best candidates here seem to be data-driven models. Also, most of the mainstream methods are well established (kriging [51], many variations of neural networks [52]–[54], radial basis functions [55], PCE [56], and so on). Unfortunately, construction of reliable models for microwave components is severely hindered by a combination of the following factors: 1) curse of dimensionality; 2) high nonlinearity of the system responses (typically, scattering parameters) both as a function of frequency and geometry/material parameters; and 3) utility demands (practically usable models have to cover sufficiently broad ranges of the system parameters and its operating conditions). Although some mitigation techniques are available, e.g., high-dimensional model representation (HDMR) [57] and orthogonal matching pursuit [58], these are of little help for general-purpose modeling of microwave components. On the other hand, alleviation of some of the aforementioned difficulties can be obtained by means of variable-fidelity approaches, such as cokriging [59], Bayesian model fusion [60], or two-stage Gaussian process regression [61].

A recently introduced concept of performance-driven modeling [62] can be considered a qualitatively different attempt to handling most of the issues discussed in the previous paragraph. It relies on identifying a region that contains high-quality designs with respect to the assumed figures of interest (e.g., allocation of operating frequencies, and power split ratios) and defining the surrogate model domain in its neighborhood. The computational benefits result from a small volume of the domain compared to the original parameter space, which translates into the improved predictive power of the surrogate even when using limited-cardinality training datasets [62]. Performance-driven modeling comes in several variations (e.g., [63] and [64]), with one of the most advanced being the nested kriging framework [65] and its generalization to variable-resolution setup [66], and dimensionality-reduced domains [67]. Notwithstanding, the advantages of the discussed methodologies are deteriorated by the necessity of defining the model domain with the use of the preoptimized reference designs. The computational cost of their acquisition may be considerable (a few hundred to over a thousand of EM simulations of the system at hand). The issue can be mitigated to a certain extent by using sensitivity data in the form of gradient-enhanced kriging (GEK) [68], which allows for reducing the number of the necessary reference points by up to 50%.

This work introduces an alternative approach to microwave component modeling. Our technique adopts the generic performance-driven concept; however, in contrast to the previous methods, it does not employ any reference designs. Instead, the surrogate model domain is determined based on a set of random observables, and an inverse regression model constructed using the EM simulation data is acquired this way. In order to capture the relevant region of the parameter space, the image of the considered objective space through the inverse model is orthogonally extended toward its normal vectors. The presented approach has a number of advantages over the prior developments: 1) the number of domain-defining observables is significantly smaller than the number of EM analyses required to obtain the reference designs, which translates into the overall smaller cost of the surrogate model setup (by up to 80%); 2) the lateral size of the domain can be automatically determined using the observable set (which was a serious problem for, e.g., the nested kriging framework [65]); and 3) the observable data can be used to complement the training samples, thereby considerably improving the model predictive power for small training sets at no extra cost. These features have been demonstrated using two examples of miniaturized microstrip couplers and a dual-band power divider.

II. Two-Stage Surrogates for Microwave Component Modeling

This section describes the fundamental components of the considered methodology. A brief recollection of the performance-driven modeling concept (see Section II-A) is followed by an introduction of the inverse regression model obtained from the random observable set (see Section II-B),

the definition of the surrogate domain (see Section II-C), and the exposition of the overall modeling flow (see Section II-D).

A. Performance-Driven Modeling Concept

This section briefly recalls the concept of performance-driven (also referred to as constrained) modeling [62], as the procedure introduced in this work exploits some of its fundamental ideas. The following notation is adopted. The vector of designable (typically, geometry) parameters of the system of interest is denoted as $\boldsymbol{x} = [x_1, \ldots, x_n]^T$. The parameter space X is determined using the lower and upper bounds for parameters, denoted as $\boldsymbol{l} = [l_1, \ldots, l_n]^T$ and $\boldsymbol{u} = [u_1, \ldots, u_n]^T$. In other words, X is an interval $[\boldsymbol{l}, \boldsymbol{u}]$ so that $l_k \leq x_k \leq u_k$ for $k = 1, \ldots, n$. For the purpose of the modeling process, we identify a number of figures of interest pertinent to the component at hand, such as its operating frequency (or frequencies in the case of multiband structures), bandwidth, power split ratio (for coupling structures), or material parameters, e.g., the dielectric permittivity of the substrate. The target values of these figures determine the design goals and allow for defining the optimality conditions for the system. These figures are denoted as f_k, $k = 1, \ldots, N$, and the interval is determined by their ranges of interest, $f_{k.\min} \leq f_k^{(j)} \leq f_{k.\max}$, $k = 1, \ldots, N$, becomes the objective space F [62]. This space becomes the (intended) region of validity of the surrogate to be constructed. For further considerations, we also use the vector notation $\boldsymbol{f} = [f_1, \ldots, f_N]^T$.

Let $U(\boldsymbol{x}, \boldsymbol{f})$ be a scalar merit function that quantifies the quality of the design $\boldsymbol{x}$ for a given objective vector $\boldsymbol{f}$ (see [65] for specific examples thereof). The function U is defined so that smaller values of $U(\boldsymbol{x}, \boldsymbol{f})$ correspond to better designs. Typically, a minimax formulation is used if the target response is unknown (e.g., matching improvement) [65] or L-square formulation if the ideal response can be identified (e.g., obtaining a specific power split ratio) [67]. The optimum design $\boldsymbol{x}^*$ is obtained for a given $\boldsymbol{f} \in F$ as

$$\boldsymbol{x}^* = U_F(\boldsymbol{f}) = \arg\min_{\boldsymbol{x}} U(\boldsymbol{x}, \boldsymbol{f}). \tag{1}$$

Then, the set of all designs that are optimum for all $\boldsymbol{f} \in F$ is denoted by

$$U_F(F) = \{U_F(\boldsymbol{f}) : \boldsymbol{f} \in F\}. \tag{2}$$

In general, $U_F(F)$ defined by (2) is an N-dimensional manifold in X. The fundamental concept behind performance-driven modeling frameworks is to construct the surrogate in a possibly small neighborhood of $U_F(F)$ because only this region contains high-quality designs [62]. Allocating the training data outside it is essentially a waste of resources. The computational benefits result from the fact that the volume of the region of interest is small compared to that of the original space X.

The central question of performance-driven methodologies is to define the surrogate model domain so that it contains $U_F(F)$. Regardless of a particular formulation (e.g., [62]–[67]), the initial estimation of the spatial allocation of the optimum design manifold is realized using a certain number of reference designs $\boldsymbol{x}^{(j)} = [x_1^{(j)}, \ldots, x_n^{(j)}]^T$, $j = 1, \ldots, p$, which are optimized w.r.t. the selected objective vectors $\boldsymbol{f}^{(j)} = [f_1^{(j)}, \ldots, f_N^{(j)}] \in F$. Because $\boldsymbol{x}^{(j)} \in U_F(F)$, the reference designs provide important information about the optimum design manifold geometry. For example, in the nested kriging framework [65], the pairs $\{\boldsymbol{f}^{(j)}, \boldsymbol{x}^{(j)}\}$, $j = 1, \ldots, p$, are employed to construct a first-level model $\boldsymbol{s}_1(\boldsymbol{f})$: $F \rightarrow X$ as an approximation of $U_F(F)$ (see Fig. 1).

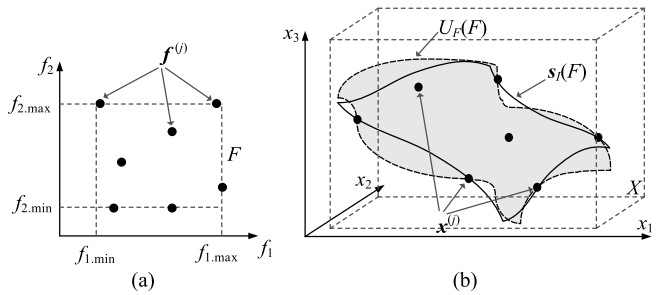

Fig. 1. Fundamental concepts of performance-driven modeling [62]. (a) Objective space F and (b) parameter space X. The reference designs are shown as black circles, whereas the optimum design manifold $U_F(F)$ is indicated as a gray surface. The first-level model image $\boldsymbol{s}_1(F)$ provides a first approximation of the manifold and has to be further extended to encapsulate the $U_F(F)$.

As demonstrated in the literature [62], [67], domain confinement in a way described above allows for a significant improvement of the model predictive power, extension of the parameter and operating condition ranges that the model is valid for, and reduction of the number of training data samples required for model identification. However, acquisition of the reference designs is a computationally expensive endeavor, which may increase the surrogate model cost in a significant manner.

In practice, the number of reference designs is between 10 and 20 [62], and the total cost of the associated optimization process may be as high as a few hundred to over a thousand EM analyses of the component at hand. Also, the acquisition process can hardly be automated because the optimization goals are scattered across the entire objective space. Some mitigation methods were proposed, either in terms of reducing the number of required designs [68] or automation of the acquisition process [69], as well as reduction of the overall cost of acquiring them [76], which alleviates the issue to a certain extent. The latter technique allows for the automated and low-cost acquisition of the reference designs required for domain definition purposes by the performance-driven frameworks. The latter technique allows for the automated and low-cost acquisition of the reference designs required for domain definition purposes by the performance-driven frameworks. The method proposed in this work can be viewed as an approach alternative to [76], with the acquisition of the reference designs abandoned altogether and replaced by allocation of random observables that subsequently serve to delimit the surrogate domain.

B. Two-Stage Inverse/Forward Modeling: Stage One

The major goal of this article is to avoid the use of reference designs while defining the domain of the surrogate model.

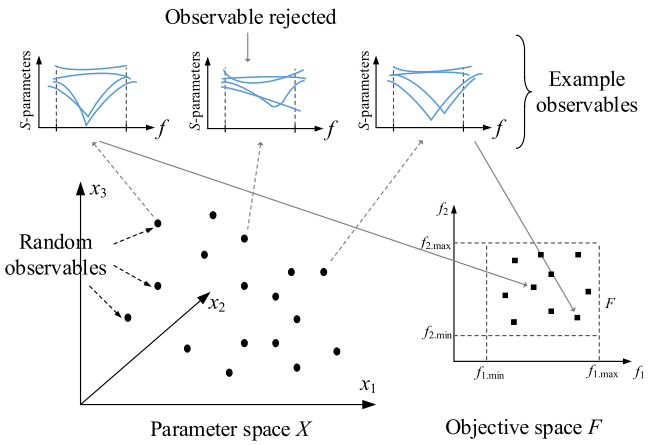

Fig. 2. Generating random observables using the example of a microstrip coupler, here, modeled over a 2-D objective space F and within a three-dimensional parameter space X. The random vectors that correspond to designs featuring operating frequency and power split ratio within F are accepted, and others are rejected. The observable set $\{\boldsymbol{x}_r^{(j)}\}_{j=1,\ldots,Nr}$, is subsequently employed to generate the inverse regression model $s_r(\cdot)$.

Here, these are replaced by a set of randomly generated parameter vectors (observables), which are preselected in terms of the associated design quality in terms of the assumed design objectives. The information contained in the observable set will be used to construct an inverse regression model providing the required approximation of the manifold $U_F(F)$.

Let us introduce the relevant notation. We denote by $\boldsymbol{x}_r^{(j)}$, $j = 1, 2, \ldots$, the aforementioned random vectors. These are generated in X using a uniform probability distribution. We also denote by $\boldsymbol{f}_r^{(j)}$ the performance figure vectors extracted from the EM-simulated system responses at $\boldsymbol{x}_r^{(j)}$. For the sake of example, let us consider a microwave coupler with the objective space consisting of its target operating frequency and the power split ratio. In this case, the two entries of the vector $\boldsymbol{f}_r^{(j)}$ may be: 1) the average value of the frequencies corresponding to the minimum of the matching and isolation characteristics ($|S_{11}|$ and $|S_{41}|$) and 2) the actual power split ratio at the above approximated operating frequency. Note that, at this stage of the modeling process, we only need to approximate the operating conditions of the system. Now, if the extracted $\boldsymbol{f}_r^{(j)}$ is within F, the random vector is accepted; it is rejected otherwise (e.g., if $\boldsymbol{f}_r^{(j)} \notin F$, or the system response is distorted so that the figures of interest cannot be extracted at all). A graphical illustration of the discussed concepts can be found in Fig. 2. The process of generating random vectors is terminated upon finding the assumed number of observables N_r (in practice, 50–100). The total number of vectors considered in the procedure is typically $2N_r$ to $3N_r$, depending on the dimensionality of the parameter space, and the ranges of the figures of interest within F. It should be noted that, if the parameter space is selected without much consideration about the expected design quality therein (e.g., with extremely broad ranges of parameters), or the circuit of interest is very sensitive to its design variables, so that even slight detuning dramatically distorts its responses, the number of random observables required to generate N_r vectors of sufficient quality might be large, thereby compromising the computational benefits of the presented method. Here, the underlying assumption is that the parameter space has not been selected *ad hoc* but at least using some basic problem-related knowledge.

Additional information is also extracted from the random vectors in the form of supplementary coefficients $p_r^{(j)}$, $j = 1, \ldots, N_r$. These coefficients are to measure the design quality (the lower the better) in order to discriminate between the vectors that are closer to the optimum design manifold $U_F(F)$ and those that are farther away from it. The former will have more impact on the inverse model discussed below. For the discussed example of the microwave coupler, assuming that the merit function U is defined to minimize $|S_{11}|$ and $|S_{41}|$ of the circuit at the operating frequency (while maintaining the power split at the required level), $p_r^{(j)}$ can be simply the maximum of $|S_{11}|$ and $|S_{41}|$ at the estimated operating frequency.

The next stage of the modeling procedure is the identification of an inverse regression model s_r: $F \rightarrow X$, which approximates the optimum design manifold $U_F(F)$, i.e., plays a role similar to that of the first-level model $\boldsymbol{s}_I$ in the nested kriging framework [67]. The inverse model maps the objective space into the parameter space X, and it is established using the training set $\{\boldsymbol{x}_r^{(j)}, \boldsymbol{f}_r^{(j)}\}_{j=1,\ldots,Nr}$. We assume the following analytical form of the model:

$$s_r(\boldsymbol{f}) = \boldsymbol{s}_r\left(\begin{bmatrix} f_1 \\ \cdots \\ f_N \end{bmatrix}\right) = \begin{bmatrix} s_{r.1}(\boldsymbol{f}) \\ \cdots \\ s_{r.n}(\boldsymbol{f}) \end{bmatrix} = \begin{bmatrix} a_{1.0} + a_{1.1}\exp\left(\sum_{k=1}^{N} a_{1.k+1} f_k\right) \\ \cdots \\ a_{n.0} + a_{n.1}\exp\left(\sum_{k=1}^{N} a_{n.k+1} f_k\right) \end{bmatrix}. \quad (3)$$

The exponential terms provide sufficient flexibility (e.g., are capable of modeling different curvatures) and are described by a few parameters. Because the primary operating conditions are frequency-related (e.g., center frequency or frequencies or the circuit), and the critical dimensions of the circuits controlling the operating frequencies are often in inversely proportional relation, it is important that the selected analytical form of the model allows for mimicking the "saturation" pertinent to $f \sim 1/L$ type of dependence (not possible using, e.g., polynomial regression).

Model identification is realized by solving the regression problems

$$\left[a_{j.0}\, a_{j.1}, \ldots, a_{j.K+1}\right] = \arg \min_{[b_0\, b_1, \ldots, b_{K+1}]} \sum_{k=1}^{N_r} w_k \left[s_{r.j}\left(\boldsymbol{f}_r^{(k)}\right) - x_{r.j}^{(k)}\right]^2 \quad (4)$$

for $j = 1, \ldots, n$. Here, $\boldsymbol{x}_r^{(k)} = [x_{r.1}^{(k)}\ x_{r.2}^{(k)}, \ldots, x_{r.n}^{(k)}]^T$, i.e., $x_{r.j}^{(k)}$ is the jth entry of $\boldsymbol{x}_r^{(k)}$, whereas the weighting factors w_k discriminate between the high- and low-quality observables.

These are assigned as

$$w_k = \left[\left(M - p_r^{(k)}\right)/M\right]^2, \quad k = 1, \ldots, N_r \quad (5)$$

where $M = \max\{k = 1, \ldots, N_r,\ j = 1, \ldots, N:\ p_r^{(k)}\}$. Recall that $p_r^{(k)}$ is the supplementary coefficients discussed before.

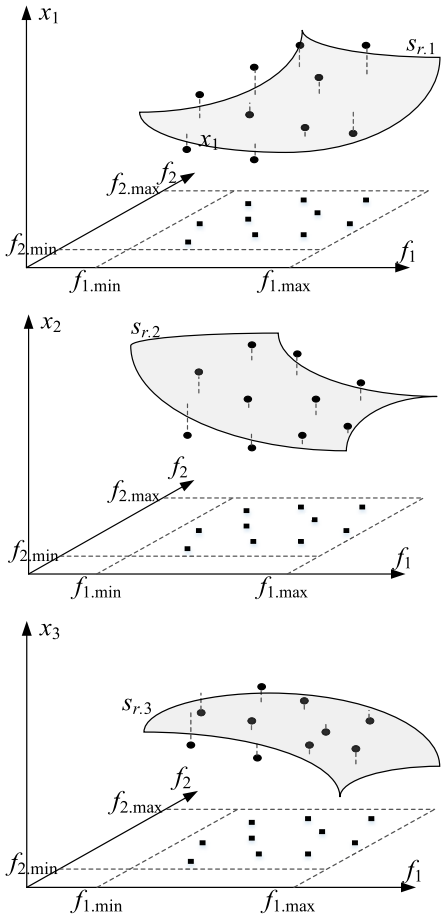

Fig. 3. Graphical illustration of the inverse regression model s_r established using random observables $\boldsymbol{x}_r^{(j)}$ and their corresponding objective vectors $\boldsymbol{f}_r^{(j)}$. The components $s_{r.j}$ of the inverse model are obtained as in (3)–(5), and their images are visualized as the gray-shaded surfaces for antenna parameters x_1 (top), x_2 (middle), and x_3 (bottom), respectively.

As $p_r^{(k)} \leq M$, the smallest weighting factor is zero (for the worst designs) and approaches one for the best ones, assuming that p_r is defined to be nonnegative. The incorporation of the weighting factors allows for the higher quality observables to have more impact on the inverse model because these designs are allocated closer to $U_F(F)$. Fig. 3 shows a graphical illustration of the inverse model in relation to the example considered in Fig. 2. It should be emphasized that a low dimensionality of the objective space F is a key factor that allows us to use low values of N_r as the inverse model is defined on F; therefore, its reliability does not depend on the dimensionality of the circuit parameter space n.

C. Two-Stage Inverse/Forward Modeling: Stage Two

Defining the domain of the final (forward) surrogate model is the next stage of the modeling process. For that, the set $s_r(F)$ (objective space image through the inverse model) has to be extended to accommodate the manifold $U_F(F)$. The extension is realized in a similar manner as in the nested kriging framework [65], i.e., using the orthonormal basis of vectors $\{\boldsymbol{v}_n^{(k)}(\boldsymbol{f})\}$, $k = 1, \ldots, n-N$, normal to $s_r(F)$ at $\boldsymbol{f}$.

The amount of extension is decided upon by the vector $\boldsymbol{T} = [T_1, \ldots, T_n]^T$ of positive real numbers. First, the extension coefficients are computed as

$$\begin{aligned}\boldsymbol{\alpha}(\boldsymbol{f}) &= \left[\alpha_1(\boldsymbol{f}), \ldots, \alpha_{n-N}(\boldsymbol{f})\right]^T \\ &= \left[\left|\boldsymbol{T}\boldsymbol{v}_n^{(1)}(\boldsymbol{f})\right|, \ldots, \left|\boldsymbol{T}\boldsymbol{v}_n^{(n-N)}(\boldsymbol{f})\right|\right]^T. \end{aligned} \quad (6)$$

It should be noted that the number of vectors $\boldsymbol{v}_n^{(k)}(\boldsymbol{f})$ normal to the image of the inverse model s_r at $\boldsymbol{f}$ is $n - N$ because the set $s_r(F)$ itself is an N-dimensional manifold in X. The coefficients α_k will determine the amount of extension toward particular normal vectors using the vector $\boldsymbol{T}$ as discussed later in this section.

The domain X_S is defined as

$$X_S = \left\{ \begin{array}{c} \boldsymbol{x} = s_r(\boldsymbol{f}) + \sum_{k=1}^{n-N} \lambda_k \alpha_k(\boldsymbol{f}) \boldsymbol{v}_n^{(k)}(\boldsymbol{f}) : \boldsymbol{f} \in F, \\ -1 \leq \lambda_k \leq 1,\ k = 1, \ldots, n-N \end{array} \right\}. \quad (7)$$

Note that X_S contains all vectors of the form of (7) for all $\boldsymbol{f} \in F$, and all $\lambda_k \in [-1, 1]$, $k = 1, \ldots, n-N$. The vectors obtained for $\lambda_k = 0$ correspond to $s_r(F)$, whereas the domain "lower" and "upper" bounds are $S_+ = \{\boldsymbol{x} \in X : \boldsymbol{x} = s_r(\boldsymbol{f}) + \sum_{k=1}^{n-N} \alpha_k(\boldsymbol{f}) \boldsymbol{v}_n^{(k)}(\boldsymbol{f})\}$ and $S_- = \{\boldsymbol{x} \in X : \boldsymbol{x} = s_r(\boldsymbol{f}) - \sum_{k=1}^{n-N} \alpha_k(\boldsymbol{f}) \boldsymbol{v}_n^{(k)}(\boldsymbol{f})\}$.

At this point, it is necessary to discuss an important difference between the nested kriging framework and the proposed approach. The former employs a scalar (i.e., parameter-independent) extension coefficient that has to be selected by the user, and the formulation of the framework does not give any indication about the "right" number (typically, selected between 0.025 and 0.1, which, more or less, corresponds to 2.5%–10% domain thickness compared to its tangential spread). An attempt to automatically determine the extension parameters has been reported in [70].

In this work, the extension factors T_j are assigned individually for each parameter. Furthermore, their values can be estimated from the observable set and the inverse surrogate, using the procedure formulated below. Consider the pair $\{\boldsymbol{x}_r^{(j)}, \boldsymbol{f}_r^{(j)}\}$. Let $P_k(\boldsymbol{x}_r^{(j)}) \in [l_k\ u_k\ ] \times F$ (a Cartesian product of the interval determined by the lower and upper bounds for the kth parameter and the objective space) be a vector minimizing the distance between $[x_{r.k}^{(j)}\ (\boldsymbol{f}_r^{(j)})^T]^T$ and $[s_{r.k}(\boldsymbol{f})\ \boldsymbol{f}^T]^T$, $\boldsymbol{f} \in F$ ($x_{r.k}^{(j)}$ stands for the kth component of the vector $\boldsymbol{x}_r^{(j)}$). In rigorous terms, we have

$$P_k\left(\boldsymbol{x}_r^{(j)}\right) = \arg\min_{\boldsymbol{f} \in F} \left\| \left[x_{r.k}^{(j)}\ \left(\boldsymbol{f}_r^{(j)}\right)^T\right]^T - \left[s_r(\boldsymbol{f})\ \boldsymbol{f}^T\right]^T \right\|. \quad (8)$$

In other words, $P_k(\boldsymbol{x}_r^{(j)})$ is the orthogonal projection of $[x_{r.k}^{(j)}\ (\boldsymbol{f}_r^{(j)})^T]^T$ onto the image of the kth component of the inverse regression model within the space $[l_k\ u_k\ ] \times F$. Furthermore, let us define

$$d_{r.k}\left(\boldsymbol{x}_r^{(j)}\right) = \left\| \left[x_{r.k}^{(j)}\ \left(\boldsymbol{f}_r^{(j)}\right)^T\right]^T - \left[s_r\left(P\left(\boldsymbol{x}_r^{(j)}\right)\right)\ P\left(\boldsymbol{x}_r^{(j)}\right)^T\right]^T \right\| \quad (9)$$

as the minimum distance between $[x_{r.k}^{(j)}\ (\boldsymbol{f}_r^{(j)})^T]^T$ and the aforementioned image; $d_{r.k}$ can be viewed as the distances

between the respective entries of the observable vectors and the gray-shaded manifolds illustrated in Fig. 3.

The extension factor T_k can be determined as

$$T_k = \frac{1}{2N_r}\sum_{j=1}^{N_r} d_{r.k}\left(\boldsymbol{x}_r^{(j)}\right). \tag{10}$$

Note that T_k is defined as half of the average distance between the kth entry of the observable vector and the respective inverse regression model manifold. The reason for choosing half of the average distance is the following. As mentioned before, the high-quality observables are allocated close to the manifold $U_F(F)$, thereby contributing in a more significant manner to identification the inverse model due to the associated weights w_k [cf. (4)]. Similarly, low-quality observables are away from $U_F(F)$. Hence, the discussed average distance provides a pessimistic estimate of the necessary domain extension (i.e., if used, the domain would also contain many mediocre designs). Consequently, reducing the extension to 50% of the average seems reasonable. This is corroborated in Section III through the application case studies. In more challenging cases (e.g., a larger number of parameters or broader parameter ranges), the aforementioned 50% can be reduced to, e.g., 25% or so.

The final surrogate model $\boldsymbol{s}(\boldsymbol{x})$ is constructed using kriging interpolation [71]. The training data are generated in X_S and denoted as $\{\boldsymbol{x}_B^{(k)}, \boldsymbol{R}(\boldsymbol{x}_B^{(k)})\}_{k=1,\ldots,NB}$, where $\boldsymbol{x}_B^{(k)} \in X_S$ are the sample points, whereas $\boldsymbol{R}$ stands for the relevant EM-evaluated system output (typically, S-parameters versus frequency). The definition of the domain X_S facilitates the sampling procedure, which is arranged in a similar way as in the nested kriging framework. More specifically, we use a bijective transformation from the unity hypercube $[0,1]^n$ onto X_S. Having $\boldsymbol{z} \in [0,1]^n$, the function h_1

$$\begin{aligned}\boldsymbol{y} = h_1(\boldsymbol{z}) &= h_1\left([z_1,\ldots,z_n]^T\right)\\ &= [f_{1.\min} + z_1(f_{1.\max} - f_{1.\min}),\ldots,f_{N.\min}\\ &\quad + z_N(f_{N.\max} - f_{N.\min})]\\ &\quad \times \left[-1+2z_{N+1},\ldots,-1+2z_n\right]\end{aligned} \tag{11}$$

maps $\boldsymbol{z}$ into $F \times [-1,1]^{n-N}$. Subsequently, the function h_2: $F \times [-1,1]^{n-N} \rightarrow X_S$

$$\begin{aligned}\boldsymbol{x} = h_2(\boldsymbol{y}) &= h_2\left([y_1,\ldots,y_n]^T\right) = s_r\left([y_1,\ldots,y_N]^T\right)\\ &\quad + \sum_{k=1}^{n-N} y_{N+k}\alpha_k\left([y_1,\ldots,y_N]^T\right)\boldsymbol{v}_n^{(k)}\left([y_1,\ldots,y_N]^T\right)\end{aligned} \tag{12}$$

maps $\boldsymbol{y}$ into X_S. Now, if $\{\boldsymbol{z}^{(k)}\}$, $k = 1,\ldots,N_B$, is a uniformly set in $[0,1]^n$ (in this work, we use a modified Latin Hypercube Sampling, LHS [72]), then the set

$$\boldsymbol{x}_B^{(k)} = H\left(\boldsymbol{z}^{(k)}\right) = h_2\left(h_1\left(\boldsymbol{z}^{(k)}\right)\right) \tag{13}$$

is uniformly distributed in X_S. It should be observed that the uniformity is understood in relation to the objective space F (not necessarily the parameter space X). This is beneficial because this type of uniformity ensures a balanced representation of objective vectors within the sample set.

1. *Random vector (observable) acquisition*: Obtain vectors $\boldsymbol{x}_r^{(j)} \in X$, $j = 1, \ldots, N_r$, along with the corresponding objective vectors $\boldsymbol{f}_r^{(j)}$ and supplementary performance coefficients $p_r^{(j)}$. The observables are generated until N_r samples are found so that $\boldsymbol{f}_r^{(j)} \in F$ for all j (cf. Section II.*B*);
2. *Inverse model construction*: Identify the inverse regression model s_r using $\{\boldsymbol{x}_r^{(j)},\boldsymbol{f}_r^{(j)}\}_{j=1,\ldots,Nr}$, as the training data set (cf. (3)), and coefficients $p_r^{(j)}$ to compute the weighting factors w_j (cf. (5));
3. *Extension vector calculation*: Obtain vector $\boldsymbol{T}$ as in (8)-(10); calculate extension coefficients $\boldsymbol{\alpha}$ (cf. (6));
4. *Surrogate model definition*: Define surrogate model domain X_S using (7);
5. *Design of experiments*: Sample domain X_S to find N_B training data points $\{\boldsymbol{x}_B^{(k)}\}_{k=1,\ldots,NB}$ (cf. (11)-(13));
6. *Training data acquisition*: Perform EM simulations to obtain system responses $\{\boldsymbol{R}(\boldsymbol{x}_B^{(k)})\}_{k=1,\ldots,NB}$;
7. *Surrogate model identification*: Identify the final surrogate $\boldsymbol{s}$ using kriging interpolation of the training samples obtained in Step 5 extended by the observable set $\{\boldsymbol{x}_r^{(k)},\boldsymbol{R}(\boldsymbol{x}_r^{(k)})\}_{k=1,\ldots,Nr}$;

Fig. 4. Two-stage inverse/forward modeling of microwave components: operational flow.

The same transformation H can also facilitate the utilization of the surrogate as a design tool. Although the geometry of the surrogate domain X_S may be complex, the processes, such as parametric optimization, can be operated from within the hypercube $[0\ 1]^n$. As the function H realizes one-to-one transformation between the unity interval and X_S, the original task $\boldsymbol{x}^* = U_F(\boldsymbol{f}) = \arg\min\{\boldsymbol{x} \in X_S : U(\boldsymbol{x},\boldsymbol{f})\}$ [cf. (1)] can be reformulated as $\boldsymbol{x}^* = U_F(\boldsymbol{f}) = \arg\min\{\boldsymbol{x} \in X_S : U(\boldsymbol{x},\boldsymbol{f})\}$, where H is used to map the vector $\boldsymbol{z}$ to X_S for surrogate model evaluation.

Note that $\boldsymbol{x}^{(0)} = s_r(\boldsymbol{f})$ is the best initial design for $\boldsymbol{f} \in F$ that can be obtained based on the available information (here, the observable set). The vector $\boldsymbol{x}^{(0)}$ can be remapped into the interval $[0\ 1]^n$ as $\boldsymbol{z}^{(0)} = H^{-1}(\boldsymbol{x}^{(0)}) = [(f_1 - f_{1.\min})/(f_{1.\max} - f_{1.\min}),\ldots,(f_N - f_{N.\min})/(f_{N.\max} - f_{N.\min})0,\ldots,0]^T$ (the last $N-n$ entries being zero).

D. Modeling Framework

Having discussed all of the basic components of the framework introduced in this work, we are in a position to describe the flow of the modeling process. There are only two user-defined parameters: the number N_r of random vectors (cf. Section II-B), typically set to 50, and the training dataset size N_B for final surrogate identification. The parameter space X and the objective space F are decided by the user depending on the intended range of validity of the model. The modeling flow has been summarized in Fig. 4. The flow diagram of the procedure can be found in Fig. 5. As mentioned before, a possibility of supplementing the

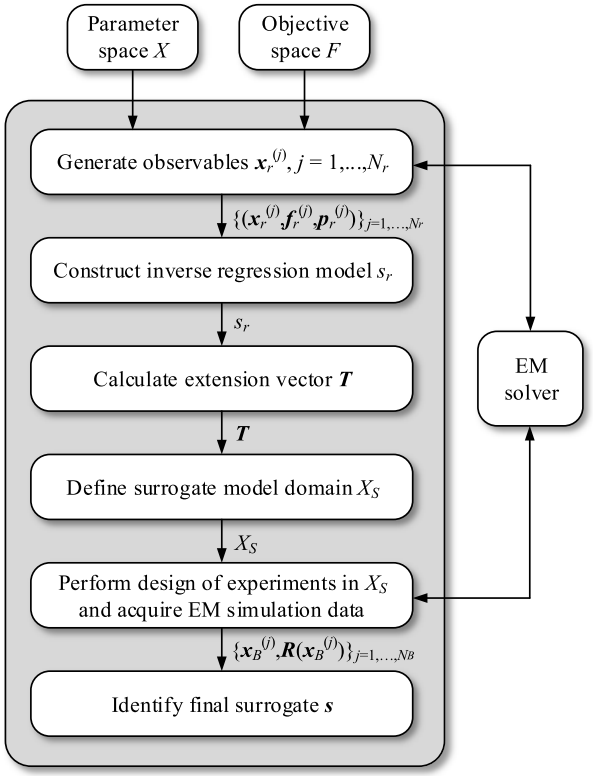

Fig. 5. Two-stage inverse/forward modeling framework: flow diagram.

training data by the observables is expected to improve the surrogate accuracy, especially for smaller datasets, which is an additional benefit of the modeling framework presented in this work.

III. Verification and Benchmarking: Case Studies

The modeling procedure described in Section II is demonstrated here using three examples of microstrip circuits, two compact couplers (rat-race and branch-line ones), and a dual-band power divider. The modeling accuracy is compared to conventional surrogates (kriging, radial basis functions, and artificial neural networks), as well as the nested kriging framework [65]. Furthermore, application examples are considered in the form of circuit optimization for selected target values of the figures of interest. The benchmarking is limited to data-driven surrogates as this is the class of models considered in this work. The advantages (e.g., a potential to construct reliable models using a small number of high-fidelity training points, as well as the suitability of local search purposes) and disadvantages (e.g., reliance on an underlying low-fidelity model or lack a universal approximation capability) of physics-based surrogates have been outlined in Section I. The mentioned disadvantages would also make it difficult to perform a proper comparison with data-driven models. In particular, setting up, e.g., space mapping metamodels, require input other than pure EM simulation data, whereas the scalability of error w.r.t. the training dataset cardinality is incomparable to that of data-driven models either due to a normally fixed number of degrees of freedom of space mapping transformations.

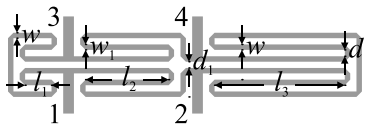

Fig. 6. Compact RRC: parameterized geometry [73].

A. Example I: Miniaturized Rat-Race Coupler

As a first example, consider a miniaturized microstrip rat-race coupler (RRC) [73], as shown in Fig. 6. The circuit is implemented on RO4003 substrate ($\varepsilon_r = 3.38$ and $h = 0.762$ mm). The independent design variables are $\boldsymbol{x} = [l_1\ l_2\ l_3\ d\ w\ w_1]^T$, whereas the remaining parameters are $d_1 = d + |w - w_1|$, $d = 1.0$, $w_0 = 1.7$, and $l_0 = 15$ fixed (all dimensions in mm). The EM model of the RRC is simulated in CST Microwave Studio.

The objective space is defined by the operating frequency f_0 of the coupler within the range from 1.0 to 2.0 GHz and the power split ratio K_P from −6 dB to 0 dB. The conventional parameter space X is defined by the lower and upper bounds $\boldsymbol{l} = [2.0\ 7.0\ 12.5\ 0.2\ 0.7\ 0.2]^T$ and the upper bounds $\boldsymbol{u} = [4.5\ 12.5\ 22.0\ 0.65\ 1.5\ 0.9]^T$. The surrogate model of the RRC S-parameters ($|S_{11}|$, $|S_{21}|$, $|S_{31}|$, and $|S_{41}|$) is to be valid over the entire objective space. The design optimality is understood as minimization of the matching and isolation characteristics at f_0, as well as maintaining the required power split ratio (also at f_0). The objective function is defined as

$$U(\boldsymbol{x}, \boldsymbol{f}) = U\left(\boldsymbol{x}, [f_0\ K_P]^T\right) = \max\{|S_{11}(\boldsymbol{x}, f_0)|, |S_{41}(\boldsymbol{x}, f_0)|\} + \beta[K_P - [|S_{21}(\boldsymbol{x}, f_0)| - |S_{31}(\boldsymbol{x}, f_0)|]]^2 \quad (14)$$

where $S_{k1}(\boldsymbol{x}, f)$ is the respective S-parameter at the design $\boldsymbol{x}$ and frequency f. The second term in (14) is a penalty function enforcing the required power split.

For verification, the two-stage surrogate model has been constructed using $N_r = 100$ random observables (obtained at the cost of 116 coupler simulations) and five different training datasets of the sizes $N_B = 50$, 100, 200, 400, and 800 samples. This allows us to investigate the predictive power scalability. As for benchmark, we use the following techniques: 1) conventional kriging interpolation model (constructed in the original parameter space X); 2) conventional RBF model (set up in the space X); 3) artificial neural network (ANN) model (feedforward network with two hidden layers, set up in the space X); and 4) nested kriging model with the thickness parameter of $T = 0.05$ (domain X_S). The last method utilized 12 reference designs with the associated acquisition cost of 779 EM simulations of the RRC. This is added to the overall expenses of setting up the surrogates.

The numerical results have been gathered in Table I. Visualization of the inverse regression model s_r for selected coupler variables can be found in Fig. 7. Note that, although the observables are spread around the inverse model surfaces due to their various levels of optimality, they are correlated and determine clear trends for geometry parameters. A comparison between EM-simulated scattering parameters of the coupler and parameters predicted by the proposed surrogate has been

TABLE I
COMPACT RRC: MODELING RESULTS AND BENCHMARKING

Number of training samples	Modeling technique									
	Kriging		RBF		ANN[&]		Nested kriging		Two-stage inverse/forward surrogate (this work)	
	Error [%]	Setup cost	Error [%]	Setup cost	Error [%]	Setup cost	Error [%]	Setup cost[$]	Error [%]	Setup cost
50	25.7	50	28.3	50	18.2	50	6.9	829	4.8	166
100	17.9	100	19.1	100	12.2	100	5.7	879	4.2	216
200	13.5	200	13.9	200	8.0	200	3.8	979	3.3	316
400	9.9	400	10.3	400	7.8	400	3.5	1,179	3.2	516
800	8.0	800	8.9	800	6.5	800	3.1	1,579	2.6	916

[$]The cost includes acquisition of the reference designs, which is 779 EM simulations of the RRC.
[#]The cost includes generation of random observables, here, 106 simulations in total to yield $N_r = 50$ accepted samples.
[&]Feedforward network with two hidden layers, trained using Levenberg-Marquardt algorithm.

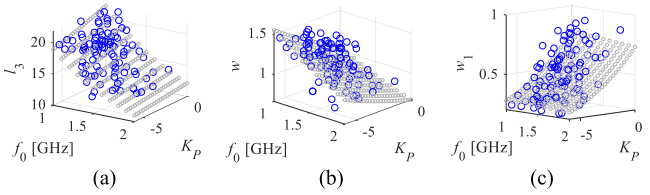

Fig. 7. Compact RRC of Fig. 6: inverse regression model for selected coupler parameters. (a) l_3, (b) w, and (c) w_1. Inverse model surfaces and random observables are shown using gray and blue circles, respectively.

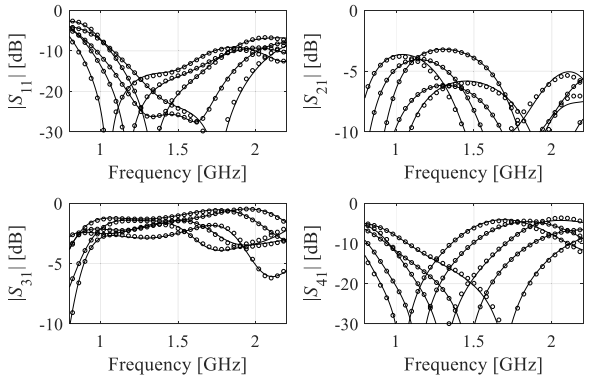

Fig. 8. Compact RRC of Fig. 6: scattering parameters at the selected test designs: EM model (—) and the proposed two-stage surrogate (o). The surrogate set up using $N_B = 400$ training samples.

shown in Fig. 8 for selected test points. An excellent agreement between the two datasets can be observed.

In this work, the modeling error is computed as a relative rms error, evaluated at the parameter vector $\boldsymbol{x}$ as $||\boldsymbol{R}_s(\boldsymbol{x}) - \boldsymbol{R}_f(\boldsymbol{x})||/||\boldsymbol{R}_f(\boldsymbol{x})||$, where $\boldsymbol{R}_s$ and $\boldsymbol{R}_f$ represent the relevant circuit responses, surrogate-predicted, and EM-simulated, respectively. Note that the predictive power of the inverse/forward surrogate discussed here is overwhelmingly superior over the conventional models (kriging, RBF, and ANN). On the other hand, it is more or less comparable to the nested kriging framework but still noticeably better for smaller training datasets of 50 and 100 samples. Although both methodologies capitalize on domain confinement, our approach allows for including all random observables into the training set, which effectively improves the accuracy. The contribution of the observables is not as pronounced for N_B exceeding 200 because of a limited number thereof.

TABLE II
COMPACT RRC: OPTIMIZATION RESULTS USING THE PROPOSED SURROGATE

Target operating conditions		Geometry parameter values [mm]					
f_0 [GHz]	K_P [dB]	l_1	l_2	l_3	d	w	w_1
1.2	0	3.74	8.88	18.53	0.42	0.95	0.78
1.5	–3	3.07	8.84	15.12	0.40	1.00	0.49
1.7	–2	3.15	8.78	13.69	0.39	0.90	0.58
1.8	0	3.48	8.15	13.56	0.32	0.77	0.72

Notwithstanding, the fundamental advantage of the proposed technique is to eliminate the need for preoptimized reference designs. As mentioned before, their acquisition cost within the nested kriging framework was almost 800 EM simulations of the RRC. At the same time, the cost of generating random observables is only 116 simulations (almost seven times cheaper). The associated computational savings are dramatic: around 80% for $N_B = 50$ and over 40% for $N_B = 800$.

In order to demonstrate the applicability of the surrogate for design purposes, the RRC has been optimized for selected target values of the operating frequency f_0 and power split ratio K_P. The numerical results are shown in Table II, whereas Fig. 9 visualizes the coupler responses at the initial and optimized designs. It can be observed that the initial designs generated by the inverse model are of good quality, and they are further improved through surrogate model optimization. At the same time, the agreement between EM simulation and surrogate-predicted scattering parameters is excellent for all considered cases.

Two of the considered designs [see Fig. 9(a) and (b)] were fabricated and experimentally validated. Fig. 10 shows the photographs of the prototypes, along with the comparison between the simulated and measured S-parameters. The agreement between the two datasets is satisfactory; minor discrepancies result from the effects of connectors not included in the computational model of the RRC.

B. Example II: Compact Branch-Line Coupler

The second validation example is a compact branch-line coupler [74], as shown in Fig. 11. The circuit is implemented on a 0.76-mm-thick substrate of the permittivity ε_r, being one of the components of the objective space. The independent parameters are $\boldsymbol{x} = [g\ l_{1\,r}\ l_a\ l_b\ w_1\ w_{2r}\ w_{3\,r}\ w_{4\,r}\ w_a\ w_b]^T$. Other variables are described by the following relations: $L = 2dL + L_s$, $L_s = 4\ w_1 + 4g + \mathrm{s} + l_a + l_b$, $W = 2dL + W_s$, $W_s = 4w_1 + 4\ g + s + 2\ w_a$, $l_1 = l_b l_{1\,r}$, $\mathrm{w}_2 = w_a w_{2\,r}$, $w_3 = w_{3\,r} w_a$, and $w_4 = w_{4\,r} w_a$. The EM model is implemented and simulated in CST Microwave Studio.

The objective space is defined by the operating frequency f_0 of the coupler within the range from 1.0 to 2.0 GHz, and the relative permittivity ε_r of the substrate the circuit is to be implemented on; the range of interest is $2.0 \leq \varepsilon_r \leq 5.0$.

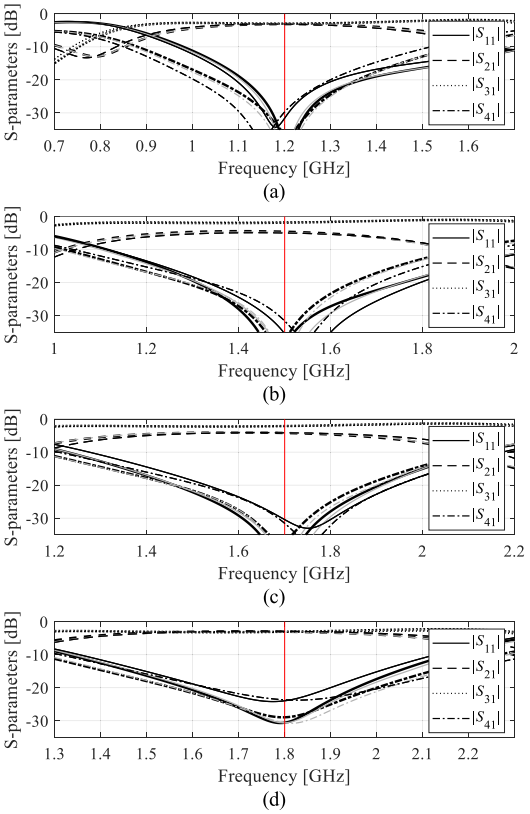

Fig. 9. Compact RRC of Fig. 6: EM-simulated S-parameters at the initial design (thin black lines) obtained using the inverse regression model, as well as surrogate (gray lines) and EM-simulated response (thick black lines) at the design obtained by optimizing the proposed two-stage surrogate set up using $N_B = 800$ training samples. The vertical lines denote the target operating frequencies. (a) $f_0 = 1.2$ GHz, and $K_P = 0$ dB, (b) $f_0 = 1.5$ GHz, and $K_P = -3$ dB, (c) $f_0 = 1.7$ GHz, and $K_P = -2$ dB, and (d) $f_0 = 1.8$ GHz, and $K_P = 0$ dB.

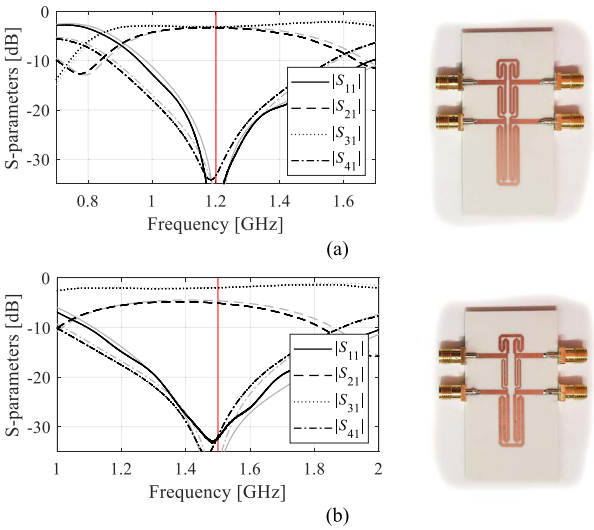

Fig. 10. Experimental validation of the RRC designs considered in Fig. 9(a) and (b). The EM simulation and measurement data are shown using gray and black lines, respectively. (a) Design optimized for $f_0 = 1.2$ GHz and $K_P = 0$ dB and (b) design optimized for $f_0 = 1.5$ GHz and $K_P = -3$ dB.

The conventional parameter space X is defined by the lower and upper bounds $\boldsymbol{l} = [0.4\ 0.43\ 5.9\ 7.7\ 0.68\ 0.28\ 0.1\ 0.1\ 2.0\ 0.2]^T$ and the upper bounds $\boldsymbol{u} = [1.0\ 0.86\ 14.0\ 16.5\ 1.5\ 0.99\ 0.65\ 0.25\ 5.5\ 0.8]^T$. The surrogate model of the

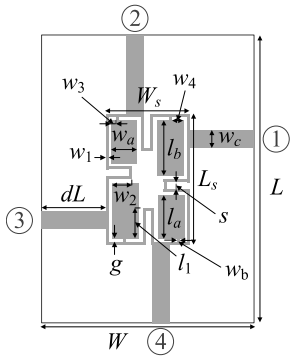

Fig. 11. Compact branch-line coupler: parameterized geometry [74].

TABLE III
COMPACT BLC: MODELING RESULTS AND BENCHMARKING

Number of training samples	Modeling technique									
	Kriging		RBF		ANN[&]		Nested kriging		Two-stage inverse/forward surrogate (this work)	
	Error [%]	Setup cost	Error [%]	Setup cost	Error [%]	Setup cost	Error [%]	Setup cost[$]	Error [%]	Setup cost
50	52.3	50	51.8	50	29.9	50	10.0	1,064	7.6	276
100	38.3	100	40.5	100	22.2	100	7.4	1,114	6.2	326
200	31.0	200	37.4	200	15.2	200	6.8	1,214	4.7	426
400	27.3	400	32.8	400	10.5	400	5.1	1,414	4.5	626
800	23.3	800	27.2	800	9.8	800	4.9	1,814	3.4	1,026

[$]The cost includes reference design acquisition, i.e., 1,014 EM simulations of the BLC.

[#]The cost includes generation of random observables, here, 226 simulations in total to yield $N_r = 50$ accepted samples.

[&]Feedforward network with two hidden layers, trained using Levenberg-Marquardt algorithm.

RRC S-parameters ($|S_{11}|$, $|S_{21}|$, $|S_{31}|$, and $|S_{41}|$) is to be valid over the entire objective space. It can be observed that the modeling task is much more challenging than for the coupler of Section III-A due to higher dimensionality of the parameter space but also broad parameter ranges. The design optimality is understood as minimization of the matching and isolation characteristics at f_0, as well as maintaining the equal power split ratio, i.e., $|S_{21}(\boldsymbol{x}, f)| = |S_{31}(\boldsymbol{x}, f)|$, also at f_0.

Our modeling framework was validated in the same way as for the previous example. We set $N_r = 100$ as the number of random observables, acquisition of which required 226 EM simulations of the BLC. The surrogates were constructed assuming $N_B = 50$, 100, 200, 400, and 800 samples. In this case, due to the challenging character of the problem, the extension parameters T_k were set to half of the values obtained from (10). For the benchmark, the same methods as in Section III.A were used: kriging, RBF, and ANN (all in conventional space X) and nested kriging [67] with the thickness parameter of $T = 0.025$ (established in the domain X_S). The nested kriging model utilizes nine reference designs, and the cost of their acquisition is 1014 EM simulations.

Table III shows the numerical results for all considered modeling techniques. The inverse model plots for the selected coupler parameter can be found in Fig. 12. Note that, for this example, the observables are more scattered and do not follow

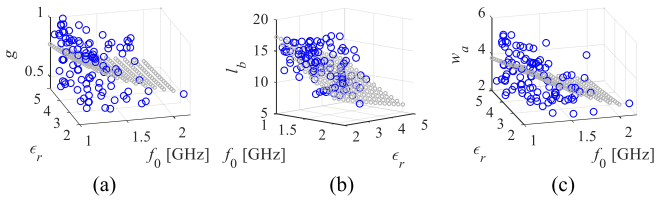

Fig. 12. Compact BLC of Fig. 11: inverse regression model for selected parameters. (a) g, (b) l_b, and (c) w_a. Inverse model surfaces and random observables are shown using gray and blue circles, respectively.

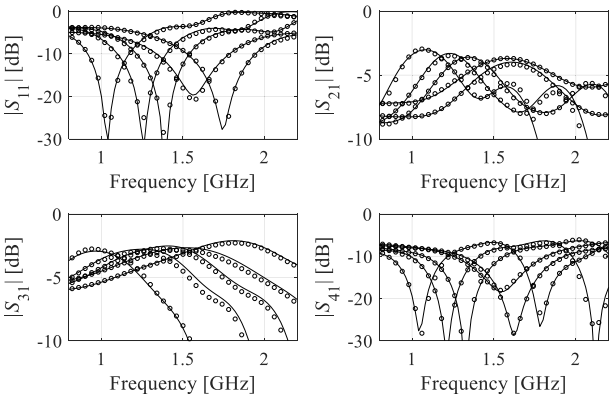

Fig. 13. Compact BLC of Fig. 11: scattering parameters at the selected test designs: EM model (—) and the proposed two-stage surrogate (o). The surrogate set up using $N_B = 400$ training samples.

TABLE IV
COMPACT BLC: OPTIMIZATION RESULTS USING THE PROPOSED SURROGATE

Target operating conditions		Geometry parameter values									
f_0 [GHz]	ε_r	g	l_{1r}	l_a	l_b	w_1	w_{2r}	w_{3r}	w_{4r}	w_a	w_b
1.0	3.0	0.85	0.60	9.05	15.2	1.06	0.71	0.40	0.20	4.76	0.54
1.2	3.0	0.77	0.60	8.84	13.4	1.17	0.56	0.39	0.18	3.90	0.54
1.5	2.5	0.69	0.61	9.03	11.7	1.20	0.65	0.41	0.18	3.54	0.53
1.7	2.5	0.64	0.61	8.94	10.9	1.21	0.61	0.41	0.19	3.18	0.55

the trends determined by the inverse surrogate, as well as for the RRC of Fig. 6, which indicates a certain parameter redundancy, typical for compact components realized using the slow wave phenomenon. Fig. 13 shows a comparison of the coupler scattering parameters predicted by the proposed surrogate and EM simulation. The results are consistent with those obtained for the RRC of Fig. 6. The two-stage inverse/forward surrogate outperforms all considered conventional surrogates. Its performance is similar to that of nested kriging, yet better for smaller training datasets, which can be explained the same way as in Section III-A: the incorporation of the observable data yields additional benefits. Finally, the computational efficiency of our approach is significantly improved over the nested kriging framework due to avoiding the usage of the reference designs. The extra cost associated with random observable generation is only 226 EM simulations, whereas the similar cost for nested kriging (reference design acquisition) is as high as the already mentioned 1014 simulations. This translates into computational savings: 74% for $N_B = 50$, 70% for $N_B = 100$, and over 43% for $N_B = 800$.

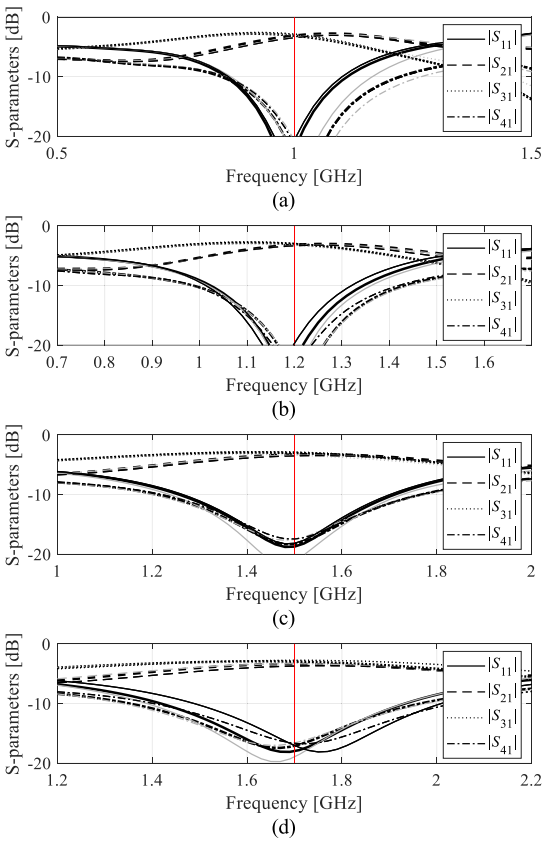

Fig. 14. Compact BLC of Fig. 11: EM-simulated S-parameters at the initial design (thin black lines) obtained using the inverse regression model, as well as surrogate (gray lines) and EM-simulated response (thick black lines) at the design obtained by optimizing the proposed two-stage surrogate set up using $N_B = 800$ training samples. The vertical lines denote the target operating frequencies. (a) $f_0 = 1.0$ GHz, and $\varepsilon_r = 3.0$, (b) $f_0 = 1.2$ GHz, and $\varepsilon_r = 3.0$, (c) $f_0 = 1.5$ GHz, and $\varepsilon_r = 2.5$, and (d) $f_0 = 1.7$ GHz, and $\varepsilon_r = 2.5$.

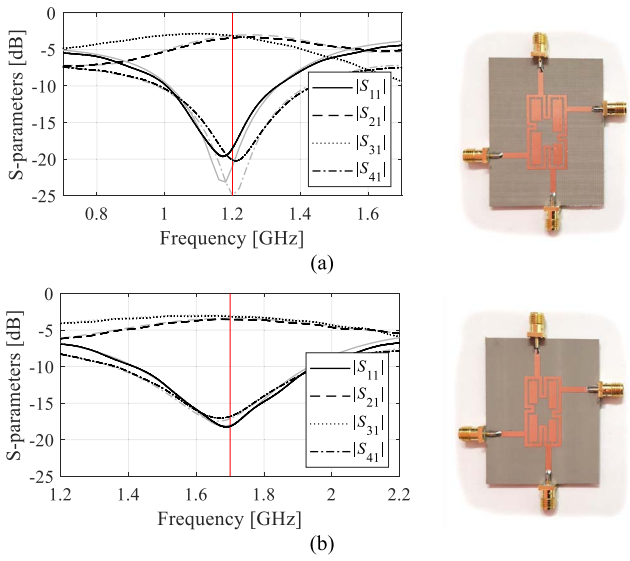

Fig. 15. Experimental validation of the BLC designs considered in Fig. 14(b) and (d). The EM simulation and measurement data are shown using gray and black lines, respectively. (a) Design optimized for $f_0 = 1.2$ GHz and $\varepsilon_r = 3.0$, and (b) design optimized for $f_0 = 1.7$ GHz and $\varepsilon_r = 2.5$.

The relevance of the considered modeling framework for design purposes has been demonstrated through several application case studies. The BLC has been optimized for

TABLE V
POWER DIVIDER: MODELING RESULTS AND BENCHMARKING

Number of training samples	Modeling technique									
	Kriging		RBF		ANN[&]		Nested kriging		Two-stage inverse/forward surrogate (this work)	
	Error [%]	Setup cost	Error [%]	Setup cost	Error [%]	Setup cost	Error [%]	Setup cost[$]	Error [%]	Setup cost
50	63.6	50	68.9	50	36.7	50	32.3	973	23.7	128
100	53.8	100	55.2	100	33.2	100	19.2	1,023	15.7	178
200	45.2	200	43.9	200	24.6	200	18.1	1,123	10.8	278
400	40.0	400	40.8	400	20.8	400	15.2	1,323	7.2	478
800	35.1	800	37.2	800	20.3	800	12.9	1,723	6.1	878

[$]The cost includes acquisition of the reference designs, which is 923 EM simulations of the divider circuit.

[#]The cost includes generation of random observables, here, 78 simulations in total to yield $N_r = 50$ accepted samples.

[&]Feedforward network with two hidden layers, trained using Levenberg-Marquardt algorithm.

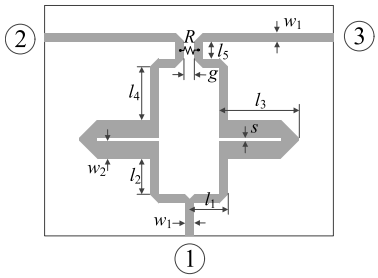

Fig. 16. Dual-band equal split power divider [75]: circuit topology; ports marked using numbers in circles. The lumped resistor is denoted as R.

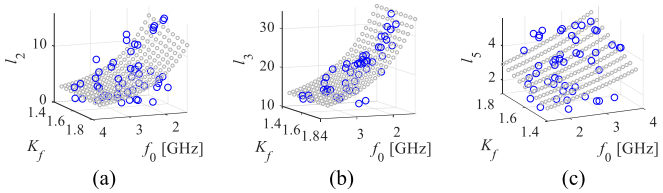

Fig. 17. Dual-band power divider of Fig. 16: inverse regression model for selected geometry parameters: (a) l_2, (b) l_3, and (c) l_5. Inverse model surfaces and random observables are shown using gray and blue circles, respectively.

several target operating frequencies and substrate permittivity, as shown in Table IV and Fig. 14. In all considered cases, the initial design obtained from the inverse model is of good quality, and the optimization process further improves the circuit responses. At the same time, the agreement between the surrogate predictions and EM-simulated data is satisfactory.

The designs considered in Fig. 14(b) and (d) were fabricated and experimentally validated. Fig. 15 shows the comparison between the simulated and measured S-parameters. The agreement between the two datasets is good; similarly, as in Fig. 10, the minor discrepancies result from the effects of connectors not included in the computational model of the coupler.

C. Example III: Dual-Band Power Divider

The third verification example is a dual-band equal-split power divider [75] (cf. Fig. 16). The circuit is implemented on AD250 substrate ($\varepsilon_r = 2.5$ and $h = 0.81$ mm). The geometry parameters are $\boldsymbol{x} = [l_1\ l_2\ l_3\ l_4\ l_5\ s\ w_2]^T$ (dimensions in mm).

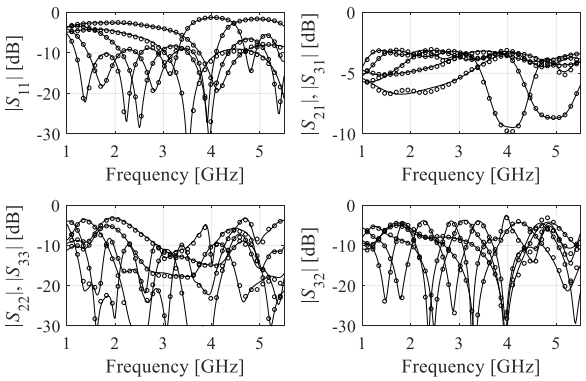

Fig. 18. Dual-band power divider of Fig. 16: scattering parameters at the selected test designs: EM model (—) and the proposed two-stage surrogate (o). The surrogate set up using $N_B = 800$ training samples.

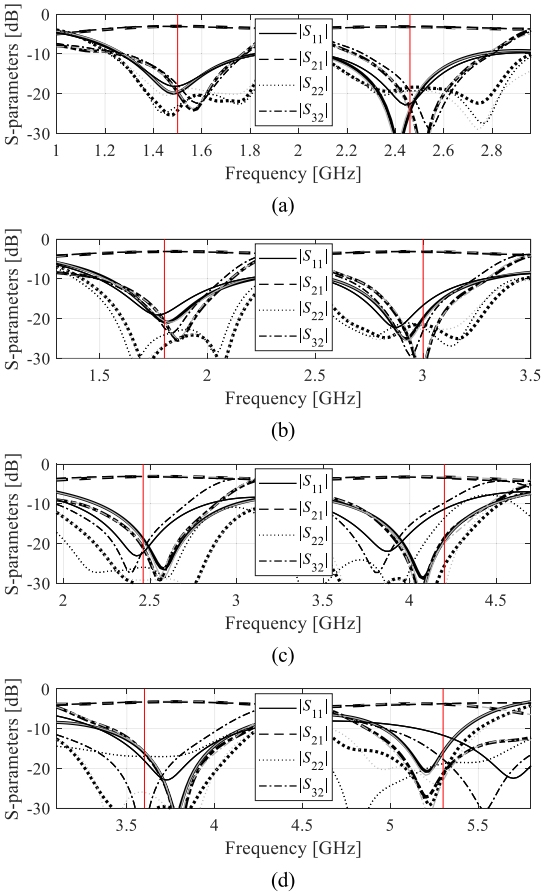

Fig. 19. Dual-band power divider of Fig. 16: EM-simulated S-parameters at the initial design (thin black lines) obtained using the inverse regression model, as well as a surrogate (gray lines) and EM-simulated response (thick black lines) at the design obtained by optimizing the proposed two-stage surrogate set up using $N_B = 800$ training samples. The vertical lines denote the target operating frequencies. (a) $f_1 = 1.5$ GHz, and $K_f = 1.63$, (b) $f_1 = 1.8$ GHz, and $K_f = 1.67$, (c) $f_1 = 2.45$ GHz, and $K_f = 1.71$, and (d) $f_1 = 3.6$ GHz, and $K_f = 1.47$.

The fixed parameters are $w_1 = 2.2$ mm (to ensure 50-Ω line impedance) and $g = 1$ mm. The EM model is implemented in CST Microwave Studio and evaluated using its time-domain solver (∼200 000 mesh cells and simulation time ∼2 min).

The objective space is defined by the frequency f_1 of the lower operating band of the divider and the ratio $K_f = f_2/f_1$ between the frequency f_2 of the upper operating band and

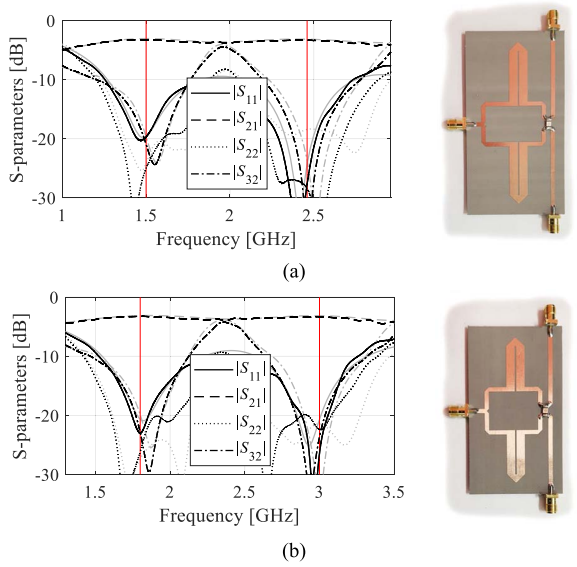

Fig. 20. Experimental validation of the power divider designs considered in Fig. 19(a) and (b). The EM simulation and measurement data are shown using gray and black lines, respectively. (a) Design optimized for $f_1 = 1.5$ GHz and $K_f = 1.63$ and (b) design optimized for $f_1 = 1.8$ GHz and $K_f = 1.67$.

TABLE VI
POWER DIVIDER: OPTIMIZATION RESULTS

Target operating conditions			Geometry parameter values [mm]						
f_1 [GHz]	K_f	$f_2 = K_f f_1$ [GHz]	l_1	l_2	l_3	l_4	l_5	s	w_2
1.5	1.63	2.45	23.4	12.4	32.8	7.35	2.58	0.63	4.51
1.8	1.67	3.0	24.0	8.88	26.9	6.68	2.95	0.70	2.25
2.45	1.71	4.2	21.4	5.10	19.3	6.33	3.18	0.79	4.22
3.6	1.47	5.3	22.5	5.77	20.5	6.26	3.32	0.83	4.32

f_1. The ranges of interest are 1.25 GHz $\leq f_1 \leq$ 4.0 GHz and $1.4 \leq K_f \leq 1.8$. The conventional parameter space X is determined by the lower bounds $\boldsymbol{l} = [14.5\ 1.1\ 13.0\ 0.5\ 1.6\ 0.19\ 3.9]^T$ and $\boldsymbol{u} = [37.0\ 16.6\ 35.0\ 15.0\ 5.6\ 1.5\ 5.8]^T$. Note that the parameter space is large with an average upper-to-lower bound ratio of nine and a maximum of 30 (for the fourth parameter).

The numerical verification setup follows that of Sections III-A and III-B. We use $N_r = 50$ observables that are obtained using 78 EM simulations of the divider structure. Due to the very challenging character of the modeling task, the extension parameters T_k were set to half of the values obtained from (10). The surrogates are identified for $N_B = 50$, 100, 200, 400, and 800. The nested kriging surrogate (one of the benchmark methods) is constructed in the domain X_S using the thickness parameter $T = 0.025$. It utilized nine reference designs with the acquisition cost of 923 EM simulations of the divider circuit. The results (Table V, Figs. 17 and 18) are consistent with those obtained for the previous examples and demonstrate the advantages of the presented modeling technique. Furthermore, even though this case is the most challenging one, the two-stage surrogate can be successfully employed for design purposes, cf. Table VI and Figs. 19 and 20.

IV. CONCLUSION

This work proposed a new two-stage technique for reduced-cost surrogate modeling of microwave components. The presented approach incorporates the concept of domain confinement, originally introduced within the performance-driven paradigm. This allows for establishing the surrogate in a restricted region of the parameters space that contains high-quality designs, and consequently, to alleviate the difficulties pertinent to the curse of dimensionality and the broad ranges of the system parameters, the model is supposed to be valid for. The surrogate model domain is defined using an auxiliary inverse regression model identified from a set of preselected random observables. The major difference between the proposed methodology and the prior performance-driven methods, including the recent nested kriging framework, is that it does not rely on preoptimized reference designs, the acquisition of which considerably increases the model setup cost.

Comprehensive verification studies, involving three microstrip devices (rat-race and branch-line couplers, as well as dual-band power divider), demonstrated the superior predictive power of the proposed two-stage surrogate, which is dramatically improved over the conventional models and comparable or better than nested kriging. The advantages of our approach are especially pronounced for smaller datasets because the very formulation of the method allows for reusing the observable data for surrogate model rendition. At the same time, the domain definition provides means for automated adjustment of its lateral dimensions (not possible for previous performance-driven methods). Finally, abandoning the concept of reference designs leads to considerable computational savings of up to 80% (for small datasets) and about 50% (for larger training ensembles). The design utility of the discussed technique has been corroborated through the application case studies and experimental validation of selected designs. The proposed approach can be considered a viable alternative to existing modeling methods, especially for challenging scenarios, such as higher dimensional parameter spaces, nonlinear system responses, broad ranges of geometry/material parameters, and operating conditions to be covered by the model validity region. Although the considered verification examples are very challenging as compared to what can normally be found in the literature, also in terms of the parameter space dimensionality, it is expected that the modeling performance might suffer for an even larger number of parameters. However, the degradation of the predictive power should be somehow mitigated by means of the two-stage approach, specifically the fact that the domain of the final surrogate is spanned by the inverse model operating from a low-dimensional objective space. One of the goals of future work will be to investigate this issue further.

ACKNOWLEDGMENT

The authors would like to thank Dassault Systemes, France, for making CST Microwave Studio available.

REFERENCES

[1] S. C. Mejillones, M. Oldoni, S. Moscato, and G. Macchiarella, "Analytical synthesis of fully canonical cascaded-doublet prototype filters," *IEEE Microw. Wireless Compon. Lett.*, vol. 30, no. 11, pp. 1017–1020, Nov. 2020.

[2] X. Tan, J. Sun, and F. Lin, "A compact frequency-reconfigurable rat-race coupler," *IEEE Microw. Wireless Compon. Lett.*, vol. 30, no. 7, pp. 665–668, Jul. 2020.

[3] P. Kurgan and S. Koziel, "Selection of circuit geometry for miniaturized microwave components based on concurrent optimization of performance and layout area," *AEU-Int. J. Electron. Commun.*, vol. 108, pp. 287–294, Aug. 2019.

[4] Z. J. Hou, Y. Yang, X. Zhu, Y. C. Li, E. Dutkiewicz, and Q. Xue, "A compact and low-loss bandpass filter using self-coupled folded-line resonator with capacitive feeding technique," *IEEE Electron Device Lett.*, vol. 39, no. 10, pp. 1584–1587, Oct. 2018.

[5] K. M. Shum, T. T. Mo, Q. Xue, and C. H. Chan, "A compact bandpass filter with two tuning transmission zeros using a CMRC resonator," *IEEE Trans. Microw. Theory Techn.*, vol. 53, no. 3, pp. 895–900, Mar. 2005.

[6] D.-S. Wu, Y. C. Li, Q. Xue, and J. Mou, "LTCC bandstop filters with controllable bandwidths using transmission zeros pair," *IEEE Trans. Circuits Syst. II, Exp. Briefs*, vol. 67, no. 6, pp. 1034–1038, Jun. 2020.

[7] Y. Dong, B. Yang, Z. Yu, and J. Zhou, "Robust fast electromagnetic optimization of SIW filters using model-based deviation estimation and Jacobian matrix update," *IEEE Access*, vol. 8, pp. 2708–2722, 2020.

[8] P. Manfredi, D. V. Ginste, D. De Zutter, and F. G. Canavero, "Generalized decoupled polynomial chaos for nonlinear circuits with many random parameters," *IEEE Microw. Wireless Compon. Lett.*, vol. 25, no. 8, pp. 505–507, Aug. 2015.

[9] Z. Ren, S. He, D. Zhang, Y. Zhang, and C. S. Koh, "A possibility-based robust optimal design algorithm in preliminary design stage of electromagnetic devices," *IEEE Trans. Magn.*, vol. 52, no. 3, Mar. 2016, Art. no. 7001504.

[10] A. K. Prasad, M. Ahadi, and S. Roy, "Multidimensional uncertainty quantification of microwave/RF networks using linear regression and optimal design of experiments," *IEEE Trans. Microw. Theory Techn.*, vol. 64, no. 8, pp. 2433–2446, Aug. 2016.

[11] B. Liu, H. Yang, and M. J. Lancaster, "Global optimization of microwave filters based on a surrogate model-assisted evolutionary algorithm," *IEEE Trans. Microw. Theory Techn.*, vol. 65, no. 6, pp. 1976–1985, Jun. 2017.

[12] H. M. Torun and M. Swaminathan, "High-dimensional global optimization method for high-frequency electronic design," *IEEE Trans. Microw. Theory Techn.*, vol. 67, no. 6, pp. 2128–2142, Jun. 2019.

[13] D.-K. Lim, K.-P. Yi, S.-Y. Jung, H.-K. Jung, and J.-S. Ro, "Optimal design of an interior permanent magnet synchronous motor by using a new surrogate-assisted multi-objective optimization," *IEEE Trans. Magn.*, vol. 51, no. 11, Nov. 2015, Art. no. 8207504.

[14] J. E. Rayas-Sánchez and V. Gutiérrez-Ayala, "EM-based Monte Carlo analysis and yield prediction of microwave circuits using linear-input neural-output space mapping," *IEEE Trans. Microw. Theory Techn.*, vol. 54, no. 12, pp. 4528–4537, Dec. 2006.

[15] X. Luo, B. Yang, and H. J. Qian, "Adaptive synthesis for resonator-coupled filters based on particle swarm optimization," *IEEE Trans. Microw. Theory Techn.*, vol. 67, no. 2, pp. 712–725, Feb. 2019.

[16] X. Li, B. Duan, J. Zhou, L. Song, and Y. Zhang, "Planar array synthesis for optimal microwave power transmission with multiple constraints," *IEEE Antennas Wireless Propag. Lett.*, vol. 16, pp. 70–73, Feb. 2017.

[17] F. Gunes, A. Uluslu, and P. Mahouti, "Pareto optimal characterization of a microwave transistor," *IEEE Access*, vol. 8, pp. 47900–47913, 2020.

[18] P.-L. Chi, H.-M. Lin, and C.-P. Chien, "A tunable balanced coupler with improved phase balance and extended bandwidth," *IEEE Access*, vol. 7, pp. 37927–37935, 2019.

[19] M. Sengupta, S. Saxena, L. Daldoss, G. Kramer, S. Minehane, and J. Cheng, "Application-specific worst case corners using response surfaces and statistical models," *IEEE Trans. Comput.-Aided Design Integr.*, vol. 24, no. 9, pp. 1372–1380, Sep. 2005.

[20] S. Koziel, S. Ogurtsov, Q. S. Cheng, and J. W. Bandler, "Rapid electromagnetic-based microwave design optimisation exploiting shape-preserving response prediction and adjoint sensitivities," *IET Microw., Antennas Propag.*, vol. 8, no. 10, pp. 775–781, 2014.

[21] S. Koziel and A. Pietrenko-Dabrowska, "Efficient gradient-based algorithm with numerical derivatives for expedited optimization of multi-parameter miniaturized impedance matching transformers," *Radioengineering*, vol. 27, no. 3, pp. 572–578, Sep. 2019.

[22] W. Zhang, F. Feng, S. Yan, W. Na, J. Ma, and Q.-J. Zhang, "EM-centric multiphysics optimization of microwave components using parallel computational approach," *IEEE Trans. Microw. Theory Techn.*, vol. 68, no. 2, pp. 479–489, Feb. 2020.

[23] F. Feng, J. Zhang, W. Zhang, Z. Zhao, J. Jin, and Q.-J. Zhang, "Coarse- and fine-mesh space mapping for EM optimization incorporating mesh deformation," *IEEE Microw. Wireless Compon. Lett.*, vol. 29, no. 8, pp. 510–512, Aug. 2019.

[24] J. E. Rayas-Sanchez, S. Koziel, and J. W. Bandler, "Advanced RF and microwave design optimization: A journey and a vision of future trends," *IEEE J. Microw.*, vol. 1, no. 1, pp. 481–493, winter 2021.

[25] Z. Zhang, H. Chen, Y. Yu, F. Jiang, and Q. S. Cheng, "Yield-constrained optimization design using polynomial chaos for microwave filters," *IEEE Access*, vol. 9, pp. 22408–22416, 2021.

[26] M. B. Yelten, T. Zhu, S. Koziel, P. D. Franzon, and M. B. Steer, "Demystifying surrogate modeling for circuits and systems," *IEEE Circuits Syst. Mag.*, vol. 12, no. 1, pp. 45–63, 1st Quart., 2012.

[27] E. Akso, İ. B. Soysal, and M. B. Yelten, "Surrogate modeling and variability analysis of on-chip spiral inductors," *Int. J. Numer. Model., Electron. Netw., Devices Fields*, vol. 31, no. 5, p. e2313, Sep. 2018.

[28] X. Xhafa and M. B. Yelten, "Design of a tunable LNA and its variability analysis through surrogate modeling," *Int. J. Numer. Model., Electron. Netw., Devices Fields*, vol. 33, no. 6, p. e2724, Nov. 2020.

[29] M. B. Yelten, P. D. Franzon, and M. B. Steer, "Surrogate-model-based analysis of analog circuits—Part II: Reliability analysis," *IEEE Trans. Device Mater. Rel.*, vol. 11, no. 3, pp. 466–473, Sep. 2011.

[30] S. Koziel, J. W. Bandler, and K. Madsen, "Space mapping with adaptive response correction for microwave design optimization," *IEEE Trans. Microw. Theory Techn.*, vol. 57, no. 2, pp. 478–486, Feb. 2009.

[31] S. Koziel, J. W. Bandler, and Q. S. Cheng, "Reduced-cost microwave component modeling using space mapping-enhanced electromagnetic-based kriging surrogates," *Int. J. Numer. Model., Electron. Netw., Devices Fields*, vol. 26, no. 3, pp. 275–286, 2013.

[32] J. Ossorio, J. C. Melgarejo, V. E. Boria, M. Guglielmi, and J. W. Bandler, "On the alignment of low-fidelity and high- fidelity simulation spaces for the design of microwave waveguide filters," *IEEE Trans. Microw. Theory Techn.*, vol. 66, no. 12, pp. 5183–5196, Dec. 2018.

[33] J. C. Melgarejo, J. Ossorio, S. Cogollos, M. Guglielmi, V. E. Boria, and J. W. Bandler, "On space mapping techniques for microwave filter tuning," *IEEE Trans. Microw. Theory Techn.*, vol. 67, no. 12, pp. 4860–4870, Dec. 2019.

[34] S. Koziel, L. Leifsson, and S. Ogurtsov, "Reliable EM-driven microwave design optimization using manifold mapping and adjoint sensitivity," *Microw. Opt. Technol. Lett.*, vol. 55, no. 4, pp. 809–813, Apr. 2013.

[35] S. Koziel, S. Ogurtsov, J. W. Bandler, and Q. S. Cheng, "Reliable space-mapping optimization integrated with EM-based adjoint sensitivities," *IEEE Trans. Microw. Theory Techn.*, vol. 61, no. 10, pp. 3493–3502, Oct. 2013.

[36] S. Koziel and S. D. Unnsteinsson, "Expedited design closure of antennas by means of trust-region-based adaptive response scaling," *IEEE Antennas Wireless Propag. Lett.*, vol. 17, no. 6, pp. 1099–1103, Jun. 2018.

[37] D. I. L. de Villiers, I. Couckuyt, and T. Dhaene, "Multi-objective optimization of reflector antennas using Kriging and probability of improvement," in *Proc. IEEE Int. Symp. Antennas Propag. USNC/URSI Nat. Radio Sci. Meeting*, San Diego, CA, USA, Jul. 2017, pp. 985–986.

[38] J. P. Jacobs, "Characterisation by Gaussian processes of finite substrate size effects on gain patterns of microstrip antennas," *IET Microw., Antennas Propag.*, vol. 10, no. 11, pp. 1189–1195, 2016.

[39] X. Yu, X. Hu, Z. Liu, C. Wang, W. Wang, and F. M. Ghannouchi, "A method to select optimal deep neural network model for power amplifiers," *IEEE Microw. Wireless Compon. Lett.*, vol. 31, no. 2, pp. 145–148, Feb. 2021.

[40] J. Yang and F. Wang, "Auto-ensemble: An adaptive learning rate scheduling based deep learning model ensembling," *IEEE Access*, vol. 8, pp. 217499–217509, 2020.

[41] J. Cai, C. Yu, L. Sun, S. Chen, and J. B. King, "Dynamic behavioral modeling of RF power amplifier based on time-delay support vector regression," *IEEE Trans. Microw. Theory Techn.*, vol. 67, no. 2, pp. 533–543, Feb. 2019.

[42] X. Wang, G. G. Wang, B. Song, P. Wang, and Y. Wang, "A novel evolutionary sampling assisted optimization method for high-dimensional expensive problems," *IEEE Trans. Evol. Comput.*, vol. 23, no. 5, pp. 815–827, Oct. 2019.

[43] A. M. Alzahed, S. M. Mikki, and Y. M. M. Antar, "Nonlinear mutual coupling compensation operator design using a novel electromagnetic machine learning paradigm," *IEEE Antennas Wireless Propag. Lett.*, vol. 18, no. 5, pp. 861–865, May 2019.

[44] J. Zhang, C. Zhang, F. Feng, W. Zhang, J. Ma, and Q.-J. Zhang, "Polynomial chaos-based approach to yield-driven EM optimization," *IEEE Trans. Microw. Theory Techn.*, vol. 66, no. 7, pp. 3186–3199, Jul. 2018.

[45] S. Koziel, "Fast simulation-driven antenna design using response-feature surrogates," *Int. J. RF Microw. Comput.-Aided Eng.*, vol. 25, no. 5, pp. 394–402, Jun. 2015.

[46] C. Zhang, F. Feng, V.-M.-R. Gongal-Reddy, Q. J. Zhang, and J. W. Bandler, "Cognition-driven formulation of space mapping for equal-ripple optimization of microwave filters," *IEEE Trans. Microw. Theory Techn.*, vol. 63, no. 7, pp. 2154–2165, Jul. 2015.
[47] S. Koziel and J. W. Bandler, "Rapid yield estimation and optimization of microwave structures exploiting feature-based statistical analysis," *IEEE Trans. Microw. Theory Techn.*, vol. 63, no. 1, pp. 107–114, Jan. 2015.
[48] S. Koziel and A. Pietrenko-Dabrowska, "Expedited feature-based quasi-global optimization of multi-band antennas with Jacobian variability tracking," *IEEE Access*, vol. 8, pp. 83907–83915, 2020.
[49] D. Gorissen, K. Crombecq, I. Couckuyt, T. Dhaene, and P. Demeester, "A surrogate modeling and adaptive sampling toolbox for computer based design," *J. Mach. Learn. Res.*, vol. 11, pp. 2051–2055, Jul. 2010.
[50] S. Marelli and B. Sudret, "UQLab: A framework for uncertainty quantification in Matlab," in *Proc. 2nd Int. Conf. Vulnerability Risk Anal. Manage. (ICVRAM)*, Liverpool, U.K.: Univ. Liverpool, Jul. 2014, pp. 2554–2563.
[51] A.-K.-S. O. Hassan, A. S. Etman, and E. A. Soliman, "Optimization of a novel nano antenna with two radiation modes using kriging surrogate models," *IEEE Photon. J.*, vol. 10, no. 4, Aug. 2018, Art. no. 4800807.
[52] Z. Liu, X. Hu, T. Liu, X. Li, W. Wang, and F. M. Ghannouchi, "Attention-based deep neural network behavioral model for wideband wireless power amplifiers," *IEEE Microw. Wireless Compon. Lett.*, vol. 30, no. 1, pp. 82–85, Jan. 2020.
[53] J. Jin, C. Zhang, F. Feng, W. Na, J. Ma, and Q.-J. Zhang, "Deep neural network technique for high-dimensional microwave modeling and applications to parameter extraction of microwave filters," *IEEE Trans. Microw. Theory Techn.*, vol. 67, no. 10, pp. 4140–4155, Oct. 2019.
[54] Z. Zhang, Q. S. Cheng, H. Chen, and F. Jiang, "An efficient hybrid sampling method for neural network-based microwave component modeling and optimization," *IEEE Microw. Wireless Compon. Lett.*, vol. 30, no. 7, pp. 625–628, Jul. 2020.
[55] P. Barmuta, F. Ferranti, G. P. Gibiino, A. Lewandowski, and D. M. M. P. Schreurs, "Compact behavioral models of nonlinear active devices using response surface methodology," *IEEE Trans. Microw. Theory Techn.*, vol. 63, no. 1, pp. 56–64, Jan. 2015.
[56] D. Spina, F. Ferranti, G. Antonini, T. Dhaene, and L. Knockaert, "Efficient variability analysis of electromagnetic systems via polynomial chaos and model order reduction," *IEEE Trans. Compon., Packag., Manuf. Technol.*, vol. 4, no. 6, pp. 1038–1051, Jun. 2014.
[57] A. C. Yucel, H. Bagci, and E. Michielssen, "An ME-PC enhanced HDMR method for efficient statistical analysis of multiconductor transmission line networks," *IEEE Trans. Compon., Packag., Manuf. Technol.*, vol. 5, no. 5, pp. 685–696, May 2015.
[58] X. Li, "Finding deterministic solution from underdetermined equation: Large-scale performance variability modeling of analog/RF circuits," *IEEE Trans. Comput.-Aided Design Integr. Circuits Syst.*, vol. 29, no. 11, pp. 1661–1668, Nov. 2010.
[59] M. C. Kennedy and A. O'Hagan, "Predicting the output from a complex computer code when fast approximations are available," *Biometrika*, vol. 87, no. 1, pp. 1–13, 2000.
[60] F. Wang *et al.*, "Bayesian model fusion: Large-scale performance modeling of analog and mixed-signal circuits by reusing early-stage data," *IEEE Trans. Comput.-Aided Design Integr. Circuits Syst.*, vol. 35, no. 8, pp. 1255–1268, Aug. 2016.
[61] J. P. Jacobs and S. Koziel, "Two-stage framework for efficient Gaussian process modeling of antenna input characteristics," *IEEE Trans. Antennas Propag.*, vol. 62, no. 2, pp. 706–713, Feb. 2014.
[62] S. Koziel and A. Pietrenko-Dabrowska, *Performance-Driven Surrogate Modeling of High-Frequency Structures*. New York, NY, USA: Springer, 2020.
[63] S. Koziel, "Low-cost data-driven surrogate modeling of antenna structures by constrained sampling," *IEEE Antennas Wireless Propag. Lett.*, vol. 16, pp. 461–464, 2017.
[64] S. Koziel and A. T. Sigurdsson, "Triangulation-based constrained surrogate modeling of antennas," *IEEE Trans. Antennas Propag.*, vol. 66, no. 8, pp. 4170–4179, Aug. 2018.
[65] S. Koziel and A. Pietrenko-Dabrowska, "Performance-based nested surrogate modeling of antenna input characteristics," *IEEE Trans. Antennas Propag.*, vol. 67, no. 5, pp. 2904–2912, May 2019.
[66] A. Pietrenko-Dabrowska and S. Koziel, "Surrogate modeling of impedance matching transformers by means of variable-fidelity electromagnetic simulations and nested cokriging," *Int. J. RF Microw. Comput.-Aided Eng.*, vol. 30, no. 8, 2020, Art. no. e22268.
[67] S. Koziel and A. Pietrenko-Dabrowska, "Low-cost data-driven modelling of microwave components using domain confinement and PCA-based dimensionality reduction," *IET Microw., Antennas Propag.*, vol. 14, no. 13, pp. 1643–1650, 2020.
[68] S. Koziel and A. Pietrenko-Dabrowska, "Low-cost performance-driven modelling of compact microwave components with two-layer surrogates and gradient kriging," *AEU-Int. J. Electron. Commun.*, vol. 126, Nov. 2020, Art. no. 153419.
[69] S. Koziel and A. Pietrenko-Dabrowska, "On computationally-efficient reference design acquisition for reduced-cost constrained modeling and re-design of compact microwave passives," *IEEE Access*, vol. 8, pp. 203317–203330, 2020.
[70] A. Pietrenko-Dabrowska and S. Koziel, "Cost-efficient surrogate modeling of high-frequency structures using nested Kriging with automated adjustment of model domain lateral dimensions," *AEU-Int. J. Electron. Commun.*, vol. 121, Jul. 2020, Art. no. 153224.
[71] A. I. J. Forrester and A. J. Keane, "Recent advances in surrogate-based optimization," *Prog. Aerosp. Sci.*, vol. 45, pp. 50–79, Jan./Apr. 2009.
[72] B. Beachkofski and R. Grandhi, "Improved distributed hypercube sampling," Amer. Inst. Aeronaut. Astronaut., Denver, CO, USA, paper AIAA 2002-1274, 2002.
[73] S. Koziel and A. T. Sigurðsson, "Performance-driven modeling of compact couplers in restricted domains," *Int. J. RF Microw. Comput.-Aided Eng.*, vol. 28, no. 6, Aug. 2018, Art. no. e21296.
[74] C. H. Tseng and C. L. Chang, "A rigorous design methodology for compact planar branch-line and rat-race couplers with asymmetrical T-structures," *IEEE Trans. Microw. Theory Techn.*, vol. 60, no. 7, pp. 2085–2092, Jul. 2012.
[75] Z. Lin and Q.-X. Chu, "A novel approach to the design of dual-band power divider with variable power dividing ratio based on coupled-lines," *Prog. Electromagn. Res.*, vol. 103, pp. 271–284, 2010.
[76] S. Koziel and A. Pietrenko-Dabrowska, "Expedited acquisition of database designs for reduced-cost performance-driven modeling and rapid dimension scaling of antenna structures," *IEEE Trans. Antennas Propag.*, vol. 69, no. 8, pp. 4975–4987, Aug. 2021, doi: 10.1109/TAP.2021.3074632.

Slawomir Koziel (Senior Member, IEEE) received the M.Sc. and Ph.D. degrees in electronic engineering from the Gdansk University of Technology, Gdansk, Poland, in 1995 and 2000, respectively, and the M.Sc. degrees in theoretical physics and in mathematics, in 2000 and 2002, respectively, and the Ph.D. degree in mathematics from the University of Gdansk, Gdansk, Poland, in 2003.

He is currently a Professor with the Department of Engineering, Reykjavik University, Iceland. His research interests include CAD and modeling of microwave and antenna structures, simulation-driven design, surrogate-based optimization, space mapping, circuit theory, analog signal processing, evolutionary computation, and numerical analysis.

Anna Pietrenko-Dabrowska (Senior Member, IEEE) received the M.Sc. and Ph.D. degrees in electronic engineering from Gdansk University of Technology, Gdansk, Poland, in 1998 and 2007, respectively.

She is currently an Associate Professor with the Gdansk University of Technology. Her research interests include simulation-driven design, design optimization, control theory, modeling of microwave and antenna structures, and numerical analysis.

Ubaid Ullah (Member, IEEE) received the M.Sc. and Ph.D. degrees in electrical and electronic engineering from the Universiti Sains Malaysia, Penang, Malaysia, in 2013 and 2017, respectively. During his Ph.D., he was awarded the Prestigious Global Fellowship and the Outstanding Student Award.

He was with Engineering Optimization and Modeling Center, School of Science and Engineering, Reykjavik University, Reykjavik, Iceland, from 2017 to 2019. He is currently an Assistant Professor with Al Ain University, Abu Dhabi Campus, United Arab Emirates. His research interests include antenna theory, small antennas, antenna polarization, dielectric resonators, waveguides, millimeter-wave antenna designs, multiple-input multiple-output (MIMO) antenna systems, EM-simulation-driven design, numerical analysis, and microwave circuit design and optimization.